

Research Article

Boosting Brain-inspired Path Integration Efficiency via Learning-based Replication of Continuous Attractor Neurodynamics

Zhangyu Ge^{†1,3}, Xu He^{†1,2,3}, Lingfei Mo^{*1,3}, Xiaolin Meng^{*1,2,3}, Wexuan Yin^{1,2,3}, Youdong Zhang^{1,2,3}, Lansong Jiang^{1,2,3}, Fengyuan Liu^{1,2,3}

Zhangyu Ge: <https://orcid.org/0009-0003-4984-0617>

Xu He: <https://orcid.org/0000-0002-7032-6618>

Lingfei Mo: <https://orcid.org/0000-0002-8561-9122>

Xiaolin Meng: <https://orcid.org/0000-0003-2440-8054>

Wenxuan Yin: <https://orcid.org/0000-0001-8556-1568>

Youdong Zhang: <https://orcid.org/0009-0000-8587-1777>

Lansong Jiang: <https://orcid.org/0009-0000-3051-8423>

Fengyuan Liu: <https://orcid.org/0009-0000-5753-8459>

1 School of Instrument Science and Engineering, Southeast University, Nanjing 210096, China

2 The China-UK Centre on Intelligent Mobility, Southeast University, Nanjing 210096, China

3 State Key Laboratory of Comprehensive PNT Network and Equipment Technology

E-mail: lfmo@seu.edu.cn & xiaolin_meng@seu.edu.cn

Abstract: The brain's Path Integration (PI) mechanism offers substantial guidance and inspiration for Brain-Inspired Navigation (BIN). However, the PI capability constructed by the Continuous Attractor Neural Networks (CANNs) in most existing BIN studies exhibits significant computational redundancy, and its operational efficiency needs to be improved; otherwise, it will not be conducive to the practicality of BIN technology. To address this, this paper proposes an efficient PI approach using representation learning models to replicate CANN neurodynamic patterns. This method successfully replicates the neurodynamic patterns of CANN-modeled Head Direction Cells (HDCs) and Grid Cells (GCs) using lightweight Artificial Neural Networks (ANNs). These ANN-reconstructed HDC and GC models are then integrated to achieve brain-inspired PI for Dead Reckoning (DR). Benchmark tests in various environments, compared with the well-known NeuroSLAM system, demonstrate that this work not only accurately replicates the neurodynamic patterns of navigation cells but also matches NeuroSLAM in positioning accuracy. Moreover, efficiency improvements of approximately 17.5% on the general-purpose device and 40~50% on the edge device were observed, compared with NeuroSLAM. This work offers a novel implementation strategy to enhance the practicality of BIN technology and holds potential for further extension.

Keywords: Brain-inspired Navigation, Path Integration, Continuous Attractor Neural Networks, Neurodynamics, Dead Reckoning

Mathematics Subject Classification: (68T40) Artificial intelligence for robotics

1. Introduction

In recent years, Brain-Inspired Navigation (BIN) research inspired by spatial cognition has attracted increasing attention and discussion within the research community. Current BIN studies draw inspiration from the brain's navigational neural mechanisms, using neurodynamic models such as Continuous Attractor Neural Networks (CANNs) to realize navigation and positioning capabilities [1]. Given that BIN research is in its nascent stage, we cannot broadly and indiscriminately model and simulate all aspects of the brain's navigation circuitry. Therefore, many current studies focus on replicating key mechanisms within the brain's navigation-related neural circuits. Among these, the neural basis of Path Integration (PI) mechanism [2] provides crucial guidance for navigation tasks, such as Dead Reckoning (DR) and Simultaneous Localization and Mapping (SLAM).

Currently, most existing BIN studies that simulate the brain's PI ability adopt the CANN-based modeling approach. These approaches deviate from the conventional logic of numerical optimization-based uncertainty estimation and reformulate it as an encoding-decoding problem of spatial experiences [3][4]. Although this paradigm is less accurate than numerical computation methods, its underlying principle resembles how the brain constructs cognitive maps [5]. It is therefore considered promising for achieving better environmental adaptability under unstructured conditions. As a result, an increasing number of researchers have devoted substantial effort to exploring its scientific value. The significance of these efforts lies in their potential to enable BIN systems to perform DR ability in non-cooperative, prior-free, and unstructured complex environments, thereby expanding the application scope of unmanned systems and intelligent robots.

Although significant transformations have occurred at both the mechanistic modeling and computational paradigm levels, the computational efficiency of CANN-modeled PI methods still requires improvement. For instance, Zheng et al. [6] observed that conventional CANN-modeled PI methods employed in the brain-inspired SLAM framework rely on cumbersome complex calculations to simulate neurodynamics. Therefore, they developed a Bayesian probabilistic framework that reformulates the CANN model into a Bayesian attractor model and integrated it into the NeuroBayesSLAM system as the PI module. Similarly, Lu et al. [7] reported the same observation in their recent work.

Of course, it is understandable that as an emerging technology, the evolution of BIN in terms of its theoretical principles, computational paradigms, and functional capabilities cannot be achieved overnight. Its capability enhancement must be realized progressively. Therefore, during this critical stage of BIN development, new ideas and methodologies can provide valuable contributions and insights to the research community of this emerging field. To this end, this paper investigates the optimization of computational efficiency in CANN-based modeling of neurodynamics. The objective is to improve the practicality of brain-inspired PI methods, thereby facilitating their deployment and integration across various edge devices and general-purpose computing platforms.

Specifically, this paper first employs Artificial Intelligence (AI)-enabled techniques to replicate the neurodynamic patterns of CANN-modeled navigation cells into lightweight Artificial Neural Networks (ANNs). Then, they are encapsulated into a brain-inspired PI framework composed of Head Direction Cells (HDCs) and Grid Cells (GCs) to realize the PI capability. Based on this design, benchmark tests are conducted to verify the representational effectiveness of the PI approach with AI-replicated CANN neurodynamics. Furthermore, this work is benchmarked against NeuroSLAM [8], a

well-known brain-inspired SLAM system, to demonstrate the validity of the proposed approach. In addition, the results show that this work achieves same performance compared to the CANN-based NeuroSLAM system in DR tasks, while improving operation efficiency by approximately 20% on workstation and 40~50% at the edge (depends on dataset).

The **main contributions** are summarized as follows:

- 1) This paper proposes a learning-based approach to replicate the CANN's neurodynamics, enabling the use of lightweight ANNs as substitutes for CANN models. This facilitates the deployment of CANN-based models and their extended functions on general-purpose computing platforms or edge devices, allowing for more efficient operation.
- 2) This paper constructs the functional models of entorhinal cortex HDCs and GCs with the AI-replicated CANN neurodynamics and integrates them into a brain-inspired PI framework to support the implementation of PI functionality, enabling DR.
- 3) Through benchmark testing with the NeuroSLAM system, which is widely recognized within the BIN field, this work developed herein achieves consistent DR performance with the NeuroSLAM system while demonstrating notable efficiency improvements on general-purpose computing devices, especially at the edge.

Outlines. Section II presents the related work, Section III details the method design and comparison, Section IV covers the experiments and evaluation, Section V includes the discussion and analysis, and Section VI concludes the paper.

2. Related work

This paper primarily focuses on the replication of the neurodynamic patterns of CANNs into representation learning-based ANNs, as well as the reconstructed modeling of navigation cells for the integration into the brain-inspired PI framework. Given that Zhang et al. [9] have already reported foundational studies on the neurodynamic modeling of CANNs, this section mainly reviews the recent state-of-the-art advances in CANN-modeled navigation cells and PI methods.

2.1 CANN-based modeling of navigation cells

Neuroscience has shown that the brain's hippocampal-entorhinal cortex neural circuit contains a large number of heterogeneous navigation cells. Their interactions form the basis of spatial cognition and navigation abilities [10]. The PI capability emerging from the complex neural networks formed by these cells is a major focus of BIN research. Over time, to simulate this, the CANN models have been widely employed for modeling key navigation cells such as pose cells [11], HDCs [12], GCs [3], and place cells [13], thereby laying the groundwork for brain-inspired PI.

Yu et al. [8], in reporting the NeuroSLAM system, provided a detailed presentation of the CANN modeling processes of HDCs and GCs in the entorhinal cortex, which is regarded as the key brain region for PI realization. This modeling method was inherited from the RatSLAM's approach of constructing CANN-based pose cell models [4][14], including local excitation, global inhibition, activity normalization, cell state updating, and decoding. The CANN modeling approaches for other types of navigation cells are largely similar and can further achieve dimensional extension of navigation cells by altering the Gaussian distribution dimensions of the CANN model.

The above typical CANN-based navigation cell modeling approach can simulate the neural activation patterns of navigation neuron clusters, enabling one-to-one mapping between the PI states and the activity states of neuron clusters through decoding. However, it exhibits considerable computational redundancy and computational complexity. As Milford et al. [15] stated, at any given time only about 1%

of the cells in the CANN model corresponding to pose cells are activated, forming an envelope (i.e., the wave packet synthesis states of 3D CANN in various dimensions) that describes the system state. Moreover, the generation of this envelope follows the processes of local excitation, global inhibition, and activity normalization, each requiring iterative computation within a recurrent framework to establish the matrix states of CANN neuronal connection strengths. In addition, the exhaustive search for the center of the envelope during the state update and decoding processes of CANNs further exacerbates the problem of low computational efficiency.

The above issues motivated Zeng et al. [6] to develop a Bayesian probabilistic framework in the NeuroBayesSLAM system to simplify CANN modeling and thus construct a more efficient PI function. The Bayesian attractor model represents the network state through Gaussian distribution parameters, rather than adhering to the neuron activation patterns of local excitation and global inhibition. Although this parametric representation simplifies the computational process, it still fails to address the efficiency issues present in decoding, and redundancy in CANN neuron activation remains.

Therefore, based on the review and analysis of the above developments, this paper proposes to employ a non-stacked structure to model key navigation cell patterns with low-dimensional CANN, and to replicate their neurodynamic properties through lightweight learning-based ANNs. On this basis, we can utilize end-to-end methods to completely reshape the modeling of neuronal activities and state decoding of navigation cells, thereby achieving high computational efficiency.

2.2 Advances in brain-inspired PI research

Numerous studies have confirmed that GCs located in the medial entorhinal cortex are critically important for the realization of PI capability. However, in the early years, since neuroscience had not yet fully elucidated the contribution and role of the entorhinal cortex in spatial cognition, the first-generation RatSLAM [14] in 2004 abstracted virtual pose cells to perform PI functionality, based solely on simulating hippocampal place cells. In the RatSLAM system, Visual Odometry (VO) estimated self-motion cues. The pose cell model, responsible for PI, encoded and decoded these cues into spatial experiences. RatSLAM then achieved Loop Closure Detection (LCD) through visual template matching (local view cells) and converted discrete spatial experiences into a topological experience map.

At present, many derivative studies have been built upon the open-sourced OpenRatSLAM project [4], which significantly advanced the development of BIN research. Many subsequent studies, including BatSLAM [16], NeuroSLAM, and among others, have been derived almost entirely from RatSLAM, sharing the common logic of simulating the operational modes of navigation cells to replicate the brain's PI capability. In addition, some researchers have raised concerns that pose cells lack physiological evidence, potentially leading to limitations in adaptability and generalization [17].

Later, with advances in neuroscience, the mechanisms of spatial cognition in the entorhinal cortex were gradually uncovered, and the role of GCs was clarified. Many researchers began to simulate the multisource information processing mechanisms of the entorhinal cortex by compiling PI information separately through HDC models and GC models, thus moving beyond the paradigm of pose cell modeling. Representative studies consistent with these characteristics can be found in [6-8, 18-21]. Subsequently, more mechanisms of navigation cells were simulated and integrated into the construction of brain-inspired PI capability. For example, Liu et al. [22] employed the CANN model to construct speed cell models and virtual distance cell models, which were combined with HDC and GC models to achieve brain-inspired PI capability in intelligent mobile applications. Moreover, some researchers have focused on the multiscale properties of navigation cells such as GCs, and on this basis developed PI models with multiscale navigation cell features, such as [20-22], which achieved certain progress.

However, it is not difficult to observe that although incorporating different functional types of navigation cells into the framework of brain-inspired PI construction provides certain capability improvements, it also significantly increases computational costs. These computational costs are positively correlated with the scale, number, dimensionality, and granularity of the navigation cell models built on CANN. Therefore, addressing the computational efficiency of CANN models is a worthy research direction, as it would enhance the practicality of brain-inspired PI models on general-purpose computing platforms and even on edge devices.

3. Method design

Figure 1 provides an overview of the efficient PI method proposed in this paper. The VO implementation adopted in this paper remains consistent with the method in NeuroSLAM, used only for estimating self-motion cues during the PI process, and thus no specific extensions are described. For details, please refer to [8].

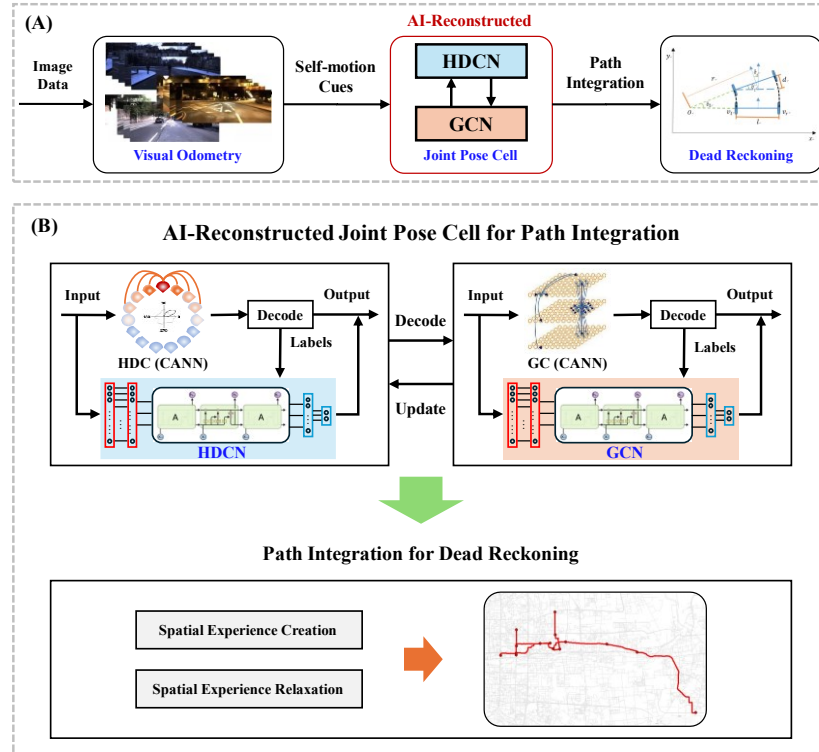


Figure 1. Framework of the proposed PI method. (A) Pipeline overview. (B) Specific representation. Where, HDCN and GCN, representing Head Direction Cell Network and Grid Cell Network respectively, are detailed in the following subsections.

Since the open-sourcing of RatSLAM, a large number of brain-inspired PI models have adopted CANN models with stacked network structures. This structure causes each virtual neuron (cell) within it to form a subset representing the neurodynamic state. The superposition of these state subsets constitutes the complete envelope (or bump) of the CANN.

As mentioned before, this modeling approach faces significant computational redundancy during state updates of the CANN model, and its decoding efficiency is low. Its computational efficiency is positively correlated with the scale, number, dimensions, and size of the navigational cell model. Therefore, when we increase the scale, size, and quantity of the navigational cell model built with CANNs, the problem of low computational efficiency becomes more pronounced. To address this challenge, this work employs a learning-based approach to fully map the neurodynamic state update pattern and decoding process of the CANN. This effectively replicates CANN's neurodynamics, and

performs a lightweight AI reconstruction of the navigational cell patterns with enhanced computational efficiency, as illustrated in Figure 1 (B).

3.1 AI reconstruction of the HDC model

By concatenating multiple 1D HDC models, we can achieve the encoding and decoding of yaw, pitch, and roll angles. This paper uses a CANN-based multi-layer HDC model to estimate the yaw and pitch angles for an efficient NeuroSLAM system, temporarily disregarding roll angle information. This is consistent with Yu et al. [8], facilitating subsequent quantitative comparison in this paper. The difference is that, since the actual correlation between height and angle is not high, two tensors are used to maintain the hidden states of the temporal layers during cell reconstruction. This allows a single ANN fitting a 1D CANN to complete the calculation of the height and angle bumps, whereas the original algorithm can be equivalent to a 2D CANN.

The design of Head Direction Cell Network (HDCN) for replicating the CANN-modeled multi-layer HDC patterns follows the lightweight principle, including an input layer, two Fully Connected (FC) layers with ReLU activation, three Long Short Term Memory (LSTM) layers, and two TimeDistributed layers for time-step state decoding. Among them, the two FC layers are used to extract abstract representations of the input sequence. To facilitate comparison with NeuroSLAM, both FC layers are set to 37 neurons. This is because the first and last neurons in the CANN model are completely equivalent, whereas in the NeuroSLAM's CANN modeling, the first and last neurons still have a spatial distance. This number setting ensures that the resolution of the reconstructed HDCN remains consistent with the neuronal encoding resolution of the HDC model in NeuroSLAM. The three LSTM layers each have 37 Units, used to fit the neurodynamic patterns of the CANN; the two TimeDistributed layers have 12 neurons and two neurons respectively, used solely for decoding the head-direction patterns learned through representation learning by the LSTM layers.

HDCN is trained with supervised learning. The training dataset for HDCN is generated by a random process that creates sequential information about angles. The randomized elements include sequence length, the pattern of angle changes, the proportion of duration for different change patterns within the entire sequence, and the value when the angle is constant. The split ratio between the training set and the validation set is 4:1, and to reduce fitting difficulty and training instability, the sequence length is controlled to 500. The sequence length of the test set is 7-10 times that of the training set, not less than 3750 frames. The input values of the sequence vary linearly within $[-\pi, \pi]$ for different patterns or are a constant value, aiming to enable the network to fit wave packet activities under different rates of change. Before the input sequence is fed into the network, one-hot encoding plus interpolation is used to obtain the input vector for the network, allowing HDCN to preemptively capture the spatial proximity relationships between different inputs, thereby reducing the fitting difficulty. This paper defines a 37-dimensional vector $x \in \{0, 1\}^{37}$ corresponding to the input of HDCN, and specifies the preference vector for HDC as:

$$V_i = OHE(i) \quad (1)$$

Where, i corresponds to the neuron index. Based on this, through interpolation, any input can be linearly mapped and transformed into a vector, as shown in formula (2):

$$V_{I_{ext}} = (1 - C_{frac})OHE(C) + C_{frac}OHE(C+1) \quad (2)$$

Where, $C = I_{ext}/2\pi * N_P$, C_{frac} refers to the fractional part of C , and N_P is the number of intervals between neurons in the 1D CANN. The external input (I_{ext}) is constrained to $[0, 2\pi)$ after a modulo operation.

The training details for HDCN are described as follows. This paper uses the decoded values of the CANN-modeled HDC as the training labels for the model. For the involved decoding methods, see formulas (7) and (8). During HDCN training, the Adam optimizer and the Mean Squared Error (MSE) loss function were adopted, training for a total of 200 epochs, with 12 sequences input per epoch.

The CANN modeling of the HDC neurodynamic pattern to be fitted is described as follows:

$$I_{ext}^i = a_{ext} \exp \left[-b_{ext} \|p_{ext} - p_i\|^2 \right] \quad (3)$$

Where, I_{ext}^i represents the stimulus input to the i th neuron. a_{ext} and b_{ext} are constants greater than 0. p_{ext} and p_i are the preferences of the external input and the i th neuron, respectively, both taken from the information state set. For example, when constructing HDC via CANN, the preference here is a certain angle within $[-\pi, \pi]$. When constructing GC, it refers to a coordinate within a specified spatial range. At this point, the neuron state update equation and the internal connection weights can be described as:

$$\tau \frac{\partial U^i(t)}{\partial t} = -U^i(t) + \rho \sum_j J_{ij} r^j(t) + I_{ext}^i(t) \quad (4)$$

Where, τ and ρ represent the synaptic time constant and neuron density, respectively. J_{ij} denotes the connection weight between the i th and j th neurons. $r^j(t)$ represents the firing rate of the j th neuron. The synaptic input $U^i(t)$ for the i th neuron can be calculated using formula (4).

$$J_{ij} = \frac{J_0}{\sqrt{2\pi}a} \exp \left[\frac{-\|p_i - p_j\|}{2a^2} \right] \quad (5)$$

The connection weights between neurons are initialized using the Gaussian function in formula (5), utilizing parameter a to control the connection range of the neurons.

$$r^i(t) = \frac{[U^i(t)]_+^2}{1 + k\rho \sum_j [U^j(t)]_+^2} \quad (6)$$

Where, $0 < k < k_c \equiv \rho J_0^2 / 8\sqrt{2\pi}a$, $[U]_+ \equiv \max(U, 0)$.

The divisive normalization in formula (6) limits the intensity of the neuronal firing rate, thereby preventing the synaptic input $U(t)$ from exhibiting an explosive growth trend. Formulas (3)-(6) complete the entire process from CANN receiving external input to wave packet state update.

In practical BIN applications, information transfer between different modules cannot be directly transmitted through abstract neural information but relies on paradigms of mathematical calculation. Therefore, it is necessary to decode the wave packet state of the CANN to obtain concrete information. For the wave packet state of a 1D CANN, its decoding formula is written as follows:

$$\theta(t) = \arctan 2 \left(\sum_i U^i(t) \sin \left(\frac{2\pi \cdot p_i}{N} \right), \sum_i U^i(t) \cos \left(\frac{2\pi \cdot p_i}{N} \right) \right) \quad (7)$$

$$y(t) = \left(\frac{\theta(t) \cdot N}{2\pi} \right) \cdot \text{mod}(Z) \quad (8)$$

Where, Z is the number of neurons in the CANN, and y represents the decoding result of the current wave packet.

3.2 AI reconstruction of the GC model

Similarly, this paper extends the 1D CANN-modeled HDC model into a 3D CANN-modeled GC model. By constructing a 3D CANN implementation, the encoding capability of GC for 3D coordinate information can be simulated. At this point, the wave packet generated by neuronal activity in the

CANN-modeled GC also transitions from the 1D ring structure of HDC to a spherical structure in 3D space. Integrating the PI update rules and decoding this spherical wave packet can simulate the GC working mode [18]. The modeling of the 3D CANN can be directly extended from the 1D CANN model. However, for a K -dimensional CANN model, assuming each dimension has N neurons, its time and space complexity are both $O(N^K)$, making the complexity of fitting the neurodynamic patterns of a 3D CANN model significantly higher than that of a 1D ones.

The design of Grid Cell Network (GCN) for replicating the CANN-modeled 3D GC patterns is the same as that of HDCN, including an Input layer, two ReLU-activated FC layers, three LSTM layers, and two TimeDistributed layers for time-step state decoding. Due to the complexity issues mentioned earlier, for multi-dimensional CANN models, this paper does not directly fit the activity states of the neurons but instead fit the vectors after dimensionality reduction and concatenation during the decoding process. The dimensionality reduction method will be introduced later. This strategy reduces both time and space complexity to $O(N \cdot K)$, which is also the key to the improved running speed of the reconstructed algorithm, and the pre-reduction wave packet state can be approximately obtained through inverse transformation.

To ensure that the resolution of GCN is consistent with HDCN to match the original NeuroSLAM settings, the number of neurons in the FC and LSTM layers of GCN are set to 111, used to replicate the neurodynamic patterns of the CANN-modeled GC. The two TimeDistributed layers have 37 neurons and 6 neurons, respectively, with every two output neurons corresponding to one dimension.

The dataset used for supervised training is also generated through a random process, identical to the random process used to generate input data for training HDCN. When creating the input sequence dataset, three 1D random sequences are pre-generated and then concatenated to simulate coordinate changes. The range of input values is still controlled within $[-\pi, \pi]$, and GCs of different scales can be mapped into this range. During input data preprocessing, this paper concatenates the input vectors calculated for the 3D coordinates according to formula (9).

$$V_I^T = [V_{x_I}^T, V_{y_I}^T, V_{z_I}^T] \quad (9)$$

The modeling process for GC is similar to that of HDC, with the difference being that the neuron preference changes from 1D angle data to a 3D vector describing coordinates. Its modeling process is shown in formulas (10) and (11):

$$\tau \frac{\partial U^i(t)}{\partial t} = -U^i(t) + \rho \sum_x \sum_y \sum_z J_{x,y,z}^i r^i(t) + I_{ext}^i(t) \quad (10)$$

$$J_{x,y,z}^i = \frac{J_0}{\sqrt{2\pi}a} \exp \left[\frac{-\|p_{x_i, y_i, z_i} - p_{x, y, z}\|}{2a^2} \right] \quad (11)$$

Where, $J_{x,y,z}^i$ represents the connection weight between the i th neuron and the neuron at spatial coordinate (x, y, z) . (x_i, y_i, z_i) represents the spatial coordinate of the i th neuron. $p_{x,y,z}$ is the preference of the neuron at spatial coordinate (x, y, z) .

The encoding and normalization process for the input sequence remains consistent with the description in HDCN. When decoding the GC wave packet, it is necessary to first sum the cell activity array according to dimensions to obtain 1D neuronal information representations on the X, Y, and Z dimensions respectively, as shown in formula (12):

$$SX(x) = \sum_y \sum_z U^{x,y,z}, SY(y) = \sum_x \sum_z U^{x,y,z}, SZ(z) = \sum_x \sum_y U^{x,y,z} \quad (12)$$

Where, SX, SY, SZ represent the 1D vectors reduced to the x, y, z dimensions, respectively. Then,

the decoded values for each dimension are calculated to obtain spatial information. Here, the concatenated result of SX , SY , SZ is the fitting target for the LSTM layer of GCN.

The training details for GCN are described as follows. This paper uses the decoded vectors from the CANN-simulated GC as the training labels for the model. These decoded vectors are concatenated from the numerator and denominator values corresponding to the arctangent calculation during the decoding of SX , SY and SZ respectively. The GCN training process is identical to the HDCN training process and will not be repeated here.

3.3 Relaxed association of spatial experiences for DR

Based on the reconstruction of HDC and GC, HDCN and GCN can directly decode the spatial experiences corresponding to the self-motion cues from the original VO input through mutual collaboration. However, it is still necessary to consider the geometric relationships between these discrete spatial experiences to form a complete PI logic, enabling the basic capability of DR, as illustrated in Figure 2.

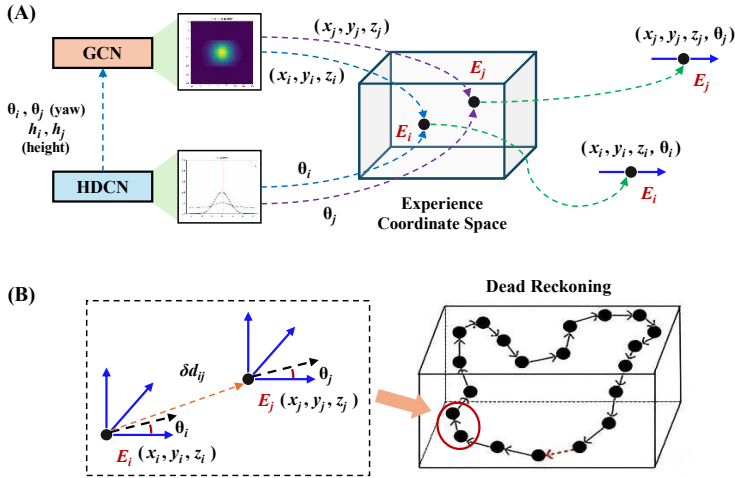


Figure 2. Illustration of relaxed association of spatial experiences decoded from the PI framework for DR.

A single spatial experience node is defined as E_i , represented by the set containing the decoded state of the joint pose estimation cells and the current pose state from VO, see (13).

$$E_i = \{P_i^{gc}, P_i^{hdc}, P_i^{exp}\} \quad (13)$$

Where, P_i^{gc} and P_i^{hdc} represent the decoded states of GCN and HDCN in the joint pose cells for the i th spatial experience, respectively, and P_i^{exp} represents the pose representation of the i th spatial experience estimated from the self-motion cues of VO. Since this paper follows the same VO implementation scheme as NeuroSLAM, the definition and connotation of P_i^{exp} are consistent with it. Details can be found in [8] and are not repeated here. Associating the joint pose estimates provided by P_i^{gc} and P_i^{hdc} with the P_i^{exp} provided by VO allows the spatial experience node to correspond to a discrete spatial state (x, y, z, θ) .

The pose of the initial spatial experience node is defined as the zero initial state. To generate a new spatial experience node, the current node must be significantly different from all existing nodes. For convenience, this paper defines P^{gc} and P^{hdc} as the decoded states concerning GCN and HDCN in the joint pose cells among all existing nodes.

This difference evaluation metric can be determined by the metric score described in formula (14).

$$S_i = \mu^{gc} |P_i^{gc} - P^{gc}| + \mu^{hdc} |P_i^{hdc} - P^{hdc}| \quad (14)$$

Where, μ^{gc} and μ^{hdc} represent the weight contributions of GCN and HDCN, respectively. If all matching scores are below a set threshold, the spatial experience node corresponding to the lowest score (i.e., the E_i corresponding to the index of $\min S_i$) is activated, representing the current PI state of the BIN system. If the current metric score exceeds a preset threshold, a new spatial experience node is generated along with a transition link associated with it. To explain this process conveniently, this paper has drawn Figure 2(B), showing the association logic from an existing spatial experience node E_i to a newly added spatial experience node E_j . This transition link stores the incremental information of the pose change δP_{ij}^{exp} , as well as the distance δd_{ij} between the two connected spatial experience nodes (i.e., the Euclidean distance of the δP_{ij}^{exp} vector).

Specifically, the calculation rule for δP_{ij}^{exp} is described as follows:

$$\delta P_{ij}^{exp} = P_j^{exp} - P_i^{exp} \quad (15)$$

On this basis, the newly added spatial experience node E_j can be represented as:

$$E_j = \{P_j^{gc}, P_j^{hdc}, P_i^{exp} + \delta P_{ij}^{exp}\} \quad (16)$$

The above spatial experience creation and update rules are the prerequisite for applying relaxation processing to all spatial experience nodes. On this basis, this paper adopts the following calculation rule to correct the pose estimate corresponding to the i th spatial experience node E_i .

$$\delta P_i^{exp} = \alpha \left| \sum_{k=1}^{N_k} (P_k^{exp} - P_i^{exp} - \delta P_{ki}^{exp}) + \sum_{t=1}^{N_t} (P_t^{exp} - P_i^{exp} - \delta P_{ti}^{exp}) \right| \quad (17)$$

Where, α is the correction rate, N_k and N_t represent the number of transitions from E_i to other spatial experience nodes, and the number of transitions from other spatial experience nodes to E_i , respectively. On this basis, integrating the above pose correction rule into the relaxation correction iteration process allows for the update of the spatial states $(x_i, y_i, z_i, \theta_i)$ corresponding to all discrete spatial experiences, forming complete PI information interpretation and generating the DR trajectory.

4. Experiment and results

To demonstrate the effectiveness of this study, experiments were conducted. NeuroSLAM was set as the baseline during the whole evaluation processes. First, a benchmark comparison was performed using the open-source dataset provided in [8]. The aim of this evaluation is to demonstrate that this work can not only reliably replicate the neurodynamic patterns of navigation cells modeled by CANNs with different dimensions, but also achieve equally instead performance to NeuroSLAM's PI framework. Furthermore, real-world testing was carried out in this paper. Moreover, practical evaluations demonstrated the computational efficiency advantages of the proposed efficient PI method. These evaluations were conducted on a Personal Computer (PC) and an edge device to showcase its practicality and transferability.

4.1 Data Preparation

The first dataset sources from Yu et al.'s NeuroSLAM work [8]. It was collected in a two-story parking garage environment, encompassing both indoor and outdoor scenes. It consists of 12583 color images with a resolution of 480*270 pixels, covering a total travel distance of approximately 600 meters. However, it lacks Ground Truth (GT) annotation. More details can be found in the original publication. The parameter configuration used on this dataset was identical to that used by Yu et al., to validate the effectiveness of the AI-replicated neurodynamic representations of navigation cells. This was done to evaluate whether this work can fully substitute the PI capability of the NeuroSLAM based on CANN modeling.

Additionally, this study collected a self-built dataset, described as follows. Representative environmental views corresponding to this dataset are shown in Figure 3. The environment is a long, narrow circular corridor with a flat floor and vertical walls. Its structure is relatively monotonous, exhibiting numerous repetitive visual features and textures with low distinctiveness. During the data collection process, pedestrians occasionally appeared suddenly in the environment, posing additional challenges to the benchmarking.

Dataset collection was performed using a mobile platform equipped with a Jetson Orin NX (16 GB) as the onboard computer. The platform runs a Linux system (Ubuntu 20.04) and data were recorded within the Robot Operating System (ROS). A RealSense D455 camera was used for image acquisition at a sampling frequency of 30 Hz and a resolution of 1280*720. During the experiment, the mobile platform moved at a constant velocity, completing one full loop along the corridor while camera images were recorded. For performance evaluation, a high precision environmental map was constructed using a high-end LiDAR sensor prior to data preparation, to generate the required GT annotations via point cloud matching results. The confidence level for these annotations is an error of ± 10 cm.

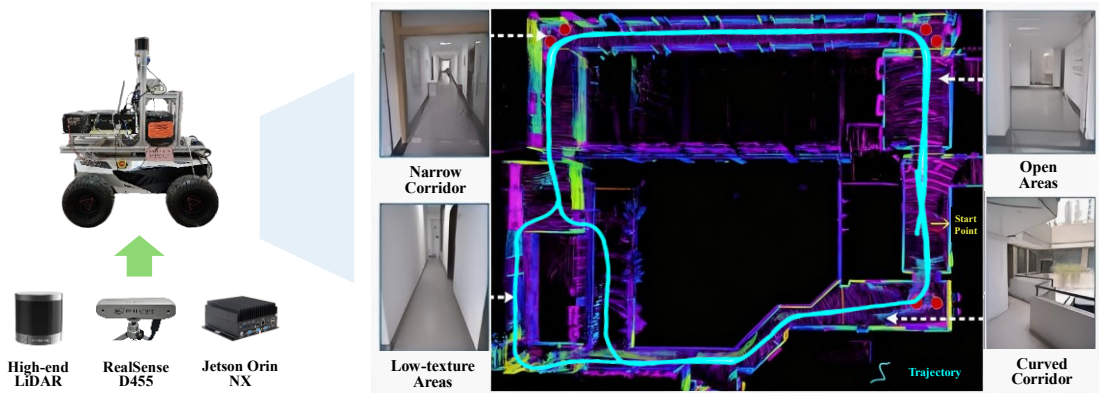


Figure 3. Data collection environment and calibration results for the self-built dataset.

4.2 Experimental conditions

Experiments in this study were conducted on both PC and edge platforms. Training of the relevant ANN models was performed on a PC equipped with one NVIDIA RTX 4060 GPU (8GB RAM) and one Intel Core i7-12650H CPU (2.7 GHz). Training data were generated using the BrainPy open-source framework [23]. The PC's software environment was configured with PyTorch 2.5.1 and Python 3.9. The edge device is a Raspberry Pi 4B (8GB RAM). Its system environment was Raspbian GNU/Linux, and the software environment was configured with Keras 2.3.1 and Python 3.7.

When evaluating on the first dataset (two-story parking garage), the parameters involved were kept consistent with the original work. The parameter configuration used on the custom dataset was tuned via an optimizer. Parameter configurations, except those related to navigation cell modeling, were shared between the original NeuroSLAM system and the proposed efficient PI method. Parameters related to navigation cell modeling remained consistent across different datasets. This approach ensures fairness in the benchmark tests.

Since the AI-reconstructed HDCN and GCN in this study no longer rely on Gaussian functions to construct the neurodynamic characteristics of CANN (such as local excitation, global inhibition, and state update), there are no corresponding parameter settings to specify. Furthermore, the parameter settings for the NeuroSLAM system used as the baseline in this paper are consistent with the configurations used in [8] and [18]. Relevant descriptions can be found in the parameter definitions and accompanying explanations provided in [8] and [18].

4.3 Experimental Results

NeuroSLAM does not strictly build its experience map frame by frame, but rather constructs the map based on spatial information representation differences at different locations. Consequently, there is only topological similarity between its experience map and the VO trajectory, preventing direct calculation of translational error against a ground truth trajectory. To enable error calculation, this study tracked the visual template update information recorded by NeuroSLAM to identify the image frames corresponding to experience map locations. This allowed for sampling and alignment of the map trajectory to compute the Mean Absolute Error (MAE) and Root Mean Square Error (RMSE).

Experiment 1: Since the first dataset lacks GT annotations, the evaluation primarily aimed to demonstrate that this work can fully replicate the neurodynamic representations of CANN-modeled PI capabilities of NeuroSLAM system.

Figure 4 visually compares the accuracy of the experience maps generated by this work and NeuroSLAM. The relevant parameter configurations have been described previously. The DR result using pure VO showed severe trajectory drift due to accumulated error after multiple loops, whereas NeuroSLAM avoided this issue and produced a stable topological experience map. According to Figure 4, the DR trajectories generated by this work and NeuroSLAM are almost completely coincident. This observation proves that this work effectively replicated the neurodynamic representations of the CANN-modeled navigation cells, achieving functional equivalence.

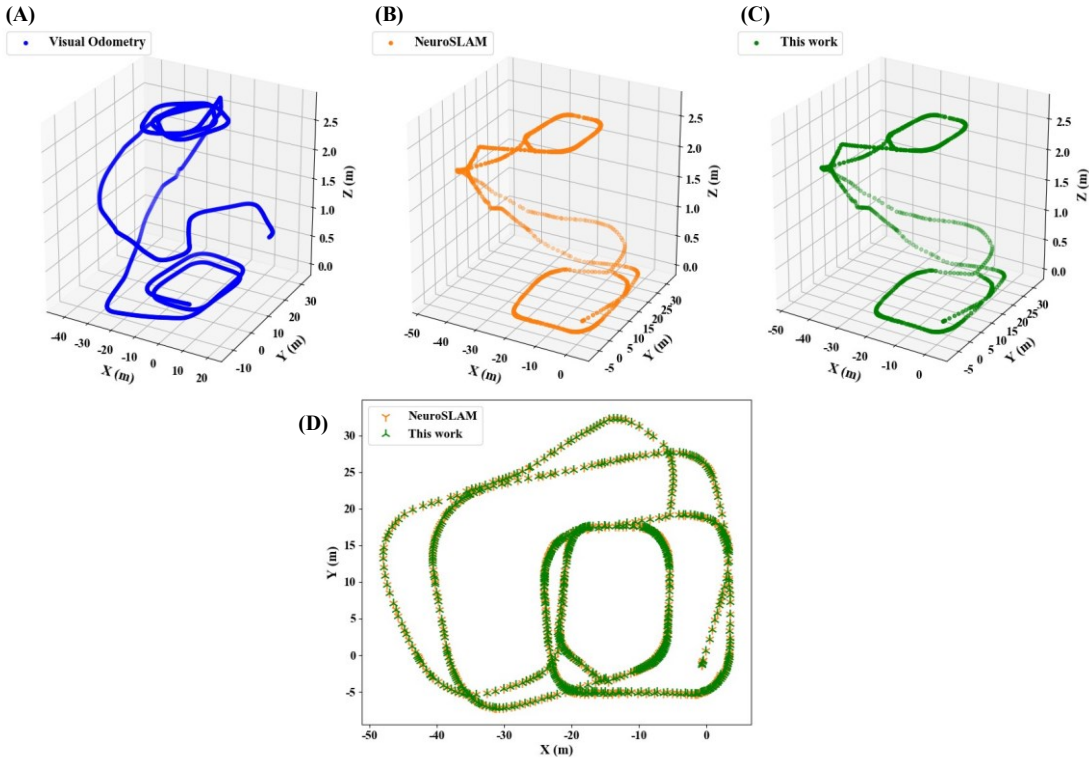


Figure 4. Accuracy comparison (Experiment 1). (A) DR trajectory from pure VO. (B) Localization trajectory from NeuroSLAM. (C) DR trajectory from this work. (D) Top-down view comparison within the same reference frame.

Moreover, compared to NeuroSLAM, the operational efficiency of this work improved by 17.5% on the PC platform. For fairness, the LCD module was excluded from NeuroSLAM during time-cost testing. Similarly, on the Raspberry Pi 4B, the operational efficiency improved by approximately 39.4%. Additionally, the involved algorithms were not quantized or subjected to computational precision truncation on either PC or a Raspberry Pi. Therefore, their accuracy remains consistent across

platforms/systems, and this will not be reiterated below to avoid redundancy.

Experiment 2: The following records the test conducted using the self-built dataset. Since this dataset possesses GT annotations with a confidence accuracy of 10 cm error. Therefore, Experiment 2 involved quantitative accuracy assessment of various methods. The GT trajectory for this dataset is shown in Figure 3. This represents a typical benchmark test with challenging settings, which is entirely different from the scenario faced in the benchmark test on the first dataset in Experiment 1.

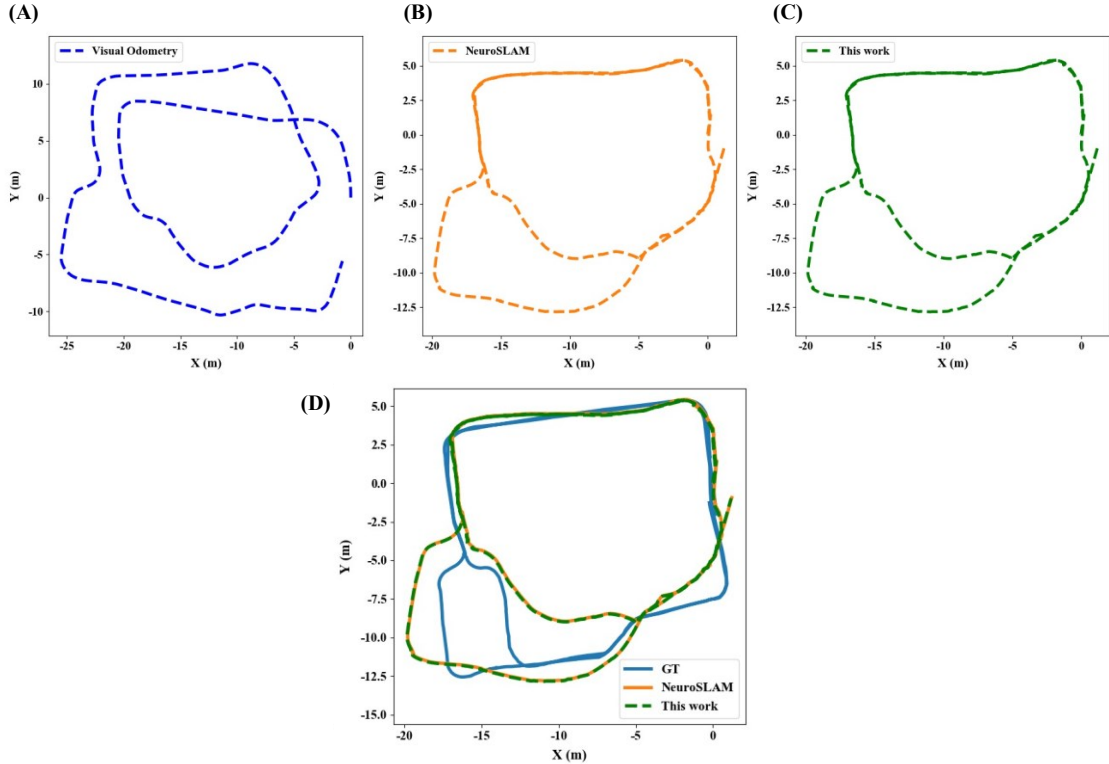


Figure 6. Accuracy comparison (Experiment 2). (A) DR trajectory from pure VO. (B) Localization trajectory from NeuroSLAM. (C) DR trajectory from this work. (D) Top-down view comparison within the same reference frame.

As shown in Figure 6, the pure VO’s trajectory did not form a closed loop. Since the test environment of Experiment 2 is rather challenging, so pure-VO drift becomes extremely severe—especially in the corridor sequence of this dataset (bottom-left panel of Figure 3), with narrow space, low light and weak texture natures.

Table 1. Trajectory Performance Comparison

	Frame	Resolution	Time Cost (s)	MAE (m)	RMSE (m)	MTE (m)
Pure VO			--	7.0	7.5	12.3
NeuroSLAM	2613	320*180	871.4 @ PC 1478.1 @ Edge	2.5	2.9	5.9
This work			743.5 @ PC 756.1 @ Edge	2.5	2.9	5.9

In contrast, the DR results from both this work and NeuroSLAM produced closed trajectories, showing much better geometric consistency with the GT trajectory. Yet, due to the severe VO drift, both NeuroSLAM and the proposed PI approach can only guarantee meter-level accuracy. However, the performance of this work and NeuroSLAM in the new test environment remained almost identical, further supporting its validity.

To ensure temporal alignment among the trajectories from different strategies, all error metrics are computed on the down-sampled sequences. Table I records the key metrics of Experiment 2. The

travelled distance of the GT trajectory is 126.4 m. Under this setting, the proposed method achieves a MAE and RMSE of the translational drift of 2.0 % and 2.3 %, respectively. The Maximum Trajectory Error (MTE) of the experience map is about 5.9 m, outperforming the VO counterpart (12.3 m). Runtime evaluations further reveal that the proposed implementation is more efficient, reducing the total execution time by 17.5 % on the PC and by 48.9% on the Raspberry Pi 4B.

5. Discussion and analysis

The traditional navigation pipeline is often described as "perception-planning/decision-control" [24]. Building capabilities at the perception level is the foundation of navigation and localization. Consequently, within the emerging field of BIN, there are numerous advances themed around brain-inspired SLAM. As analyzed in Section II, simulating the PI capability of the entorhinal cortex is a core component in almost all existing brain-inspired SLAM systems based on CANNs. Essentially, the core logic of PI involves integrating internal and external cues captured by the BIN system by simulating the collaborative logic between GCs and other navigation cells, thereby forming spatial experiences. How to effectively utilize the spatial experiences generated by PI is the primary concern for BIN systems.

Therefore, simulating PI capability is a core mechanism of brain-inspired SLAM but is not limited to the SLAM topic. For instance, Edwards et al. [25], 26] utilized CANNs to simulate the PI capability of GCs for vector-based navigation tasks. Yang et al. [20] directly implemented a DR task with a CANN-based multi-scale GC model to build PI capability, without involving loop closure detection as in SLAM. The method developed in this study also focuses on realizing PI capability, aiming to achieve the DR capability for BIN systems directly.

After clarifying the essence of simulating the brain's PI capability, we need to consider its modeling effectiveness and computational efficiency. The former aims to enable the BIN system to achieve a more comprehensive replication of the brain's PI capability, while the latter is pursued to promote the practicality of brain-inspired PI models. Among existing studies on simulating brain-inspired PI capability, most advances belong to the former category, whereas the work presented herein belongs to the latter.

Section 4 has conducted benchmark tests after implementing the approach of replicating CANN's neurodynamics using lightweight ANNs. Apart from the PI capability, the main difference between this work and the NeuroSLAM system lies in the LCD. In Experiment 1, the open-source data from the NeuroSLAM work was used. Debug its original code, we reveal that, under its default parameters, the influence of its LCD capability on the construction of the experience map is relatively weak. As for Experiment 2, we likewise noticed this issue on our self-collected dataset, that is, the LCD component of NeuroSLAM did not perform the expected map correction.

After meticulous step-by-step code debugging, we suspect the reason might be that the parameter configuration for this dataset was not optimally tuned, leading to short durations for successful visual template matching (triggering effective energy injection) and a very small intervention impact during continuous energy injection. Therefore, on this dataset, the relaxation and association process within NeuroSLAM's experience map played the dominant role in modifying and adjusting the spatial experience. Consequently, the DR trajectories from both methods almost completely overlapped, enabling this work to achieve results on par with NeuroSLAM, despite lacking LCD.

Moreover, given that Section 4 only presented functional tests of the proposed efficient brain-inspired PI method without analyzing the neural activity patterns of the navigation cells, this section provides supplementary analysis.

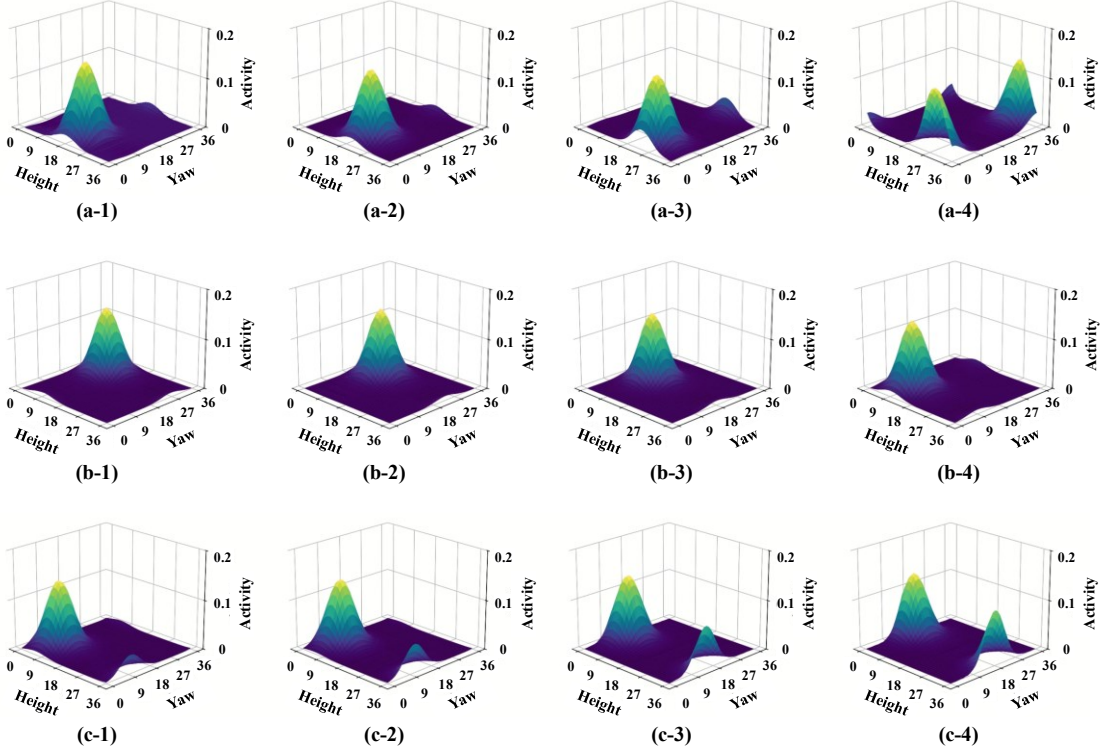


Figure 8. Neural activity patterns decoded from the HDCN. (a-1) to (a-4): rising height. (b-1) to (b-4): unchanged height. (c-1) to (c-4): falling height.

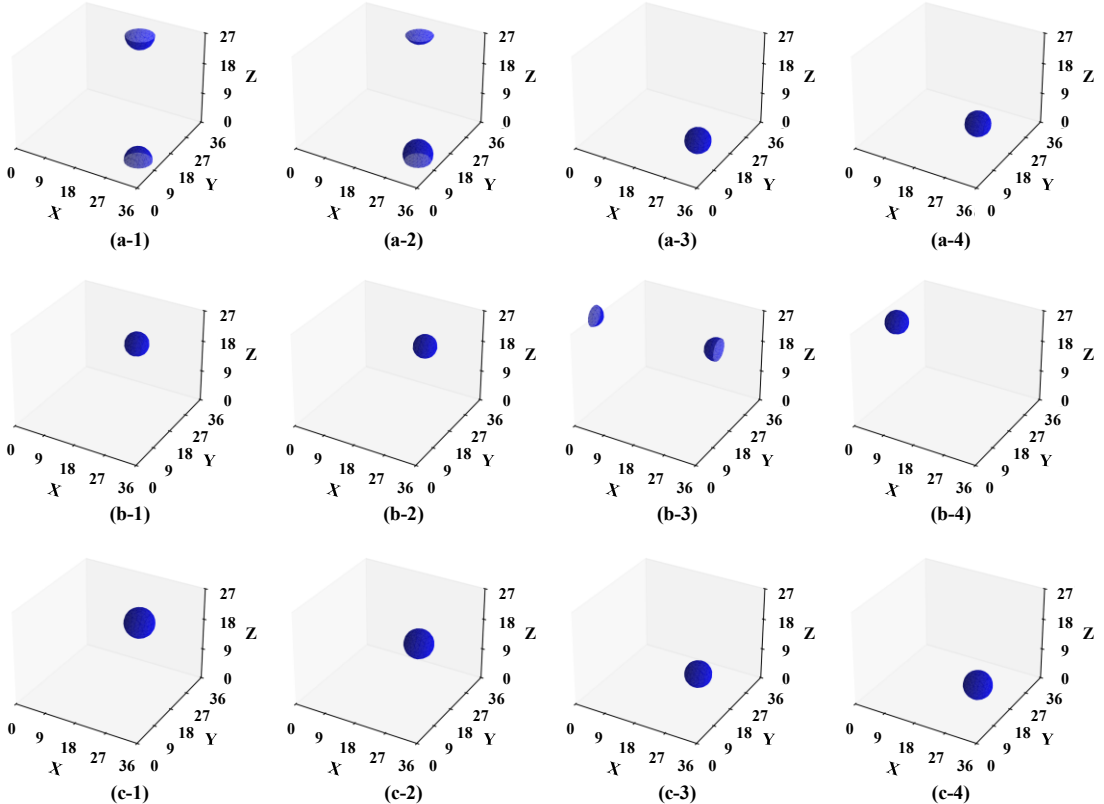


Figure 9. Neural activity patterns decoded from the GCN. (a-1) to (a-4): rising height. (b-1) to (b-4): unchanged height. (c-1) to (c-4): falling height.

Figure 8 shows the changes in the neurodynamics of the AI-reconstructed HDCN during changes in altitude. When the system's altitude state changes, as shown in panels (a-1) to (a-4) and (c-1) to (c-4), the activity bump state decoded from the HDCN undergoes corresponding smooth movement along the

altitude dimension. When the bump exceeds the boundary range, the HDCN can excite neighboring neurons on the opposite side, allowing the bump state to transition continuously and smoothly, fully replicating the activity continuity of CANN. When the system altitude remains constant, the bump state decoded from the HDCN remains stable in altitude and continues to move along the yaw dimension, as demonstrated in the groups (b-1) to (b-4) in Figure 8.

Figure 9 shows the bump activation patterns decoded from the GCN under different altitude change modes. As shown in panels (a-1) to (a-4) and (c-1) to (c-4), when the altitude changes, the bump moves according to the trend of altitude change. When the cumulative change exceeds the representational range, the bump, similar to the HDC, activates neighboring neurons on the opposite side, exhibiting the continuous, stable, and periodic activity pattern characteristic of CANN. When the altitude is unchanged, as shown in panels (b-1) to (b-4) in Figure 9, the bump activity decoded from the GCN remains stable on the Z axis and moves along the X axis, crossing boundaries.

From the above analysis, we can qualitatively conclude that the learning-based approach for replicating CANN's neurodynamics proposed in this paper is successful. However, the specific CANN modeling method adopted here is not the most advanced. For instance, many novel CANN modeling methods have been reported in recent years, such as [27, [28]. Therefore, this work has room for further extension, and we believe it is worthwhile to explore its application to more comprehensive CANN modeling methods. Furthermore, the lightweight nature of this work renders its quantization and acceleration on edge AI chips, and even deployment on neuromorphic hardware via ANN2SNN transformation [29], as promising directions for future exploration.

6. Conclusion

This paper presents an efficient brain-inspired PI method by replicating the neurodynamic representations of CANNs using lightweight ANNs. This method avoids computational redundancy in the RatSLAM-derived PI modeling, enhancing efficiency. It achieved roughly 17.5% efficiency gains on general-purpose devices and 40~50% on edge devices compared to the well-known NeuroSLAM. Overall, the benchmark tests, shown in Section 4, consistently reported performance equivalent to NeuroSLAM. Moreover, on this basis, the computational efficiency improvement brought by this work also demonstrates its value, particularly for applications on edge devices. Thereby, it promotes the practicality of BIN technology.

In the future, we hope to go beyond the existing ideas and replicate the neurodynamic characteristics of navigation cells modeled by more advanced CANN models. Moreover, building PI capability is a core issue for brain-inspired SLAM systems, but this paper has currently only explored the brain-inspired PI method itself, achieving DR capability. The future research directions encompass integrating this work into a complete SLAM pipeline with effective loop closure detection strategies, and investigating its deployment potential on edge AI accelerators and neuromorphic chips. In summary, this paper provides a feasible path to realizing a scalable and efficient BIN system, with the potential for practicality and continuous expansion.

Acknowledgments

This work is mainly sponsored by Natural Science Foundation of Jiangsu Province under Grant No. BK20243064. Xu He receives support from the Postgraduate Research & Practice Innovation Program of Jiangsu Province (Grant numbers: SJCX24_0067) & SEU Innovation Capability Enhancement Plan for Doctoral Students (Grant numbers: CXJH_SEU 24204).

Conflict of interest statement

The authors declare that they have no competing interests.

References

- [1] Bai, Y., Shao, S., et al. A review of brain-inspired cognition and navigation technology for mobile robots. *Cyborg and Bionic Systems*. 2024; 5: 0128.
- [2] McNaughton, B.L., Battaglia, F.P., et al. Path integration and the neural basis of the ‘cognitive map’. *Nature Reviews Neuroscience*. 2006; 7(8): 663-678.
- [3] Milford, M., Wiles, J., et al. Solving navigational uncertainty using grid cells on robots. *PLoS Computational Biology*. 2010; 6(11): e1000995.
- [4] Ball, D., Heath, S., et al. (2013). OpenRatSLAM: an open source brain-based SLAM system. *Autonomous Robots*. 2013; 34(3): 149-176.
- [5] Yuan, M., Tian, B., et al. An entorhinal-hippocampal model for simultaneous cognitive map building. *AAAI Conference on Artificial Intelligence (AAAI)*. 2015; 586-592.
- [6] Zeng, T., Tang, F., et al. NeuroBayesSLAM: neurobiologically inspired Bayesian integration of multisensory information for robot navigation. *Neural Networks*. 2020; 126: 21-35.
- [7] Lu, T., Wang, Z., et al. (2025). Hybrid-NeuroSLAM: a neurobiologically inspired hybrid visual-inertial SLAM method for large scale environment. *IEEE Robotics and Automation Letters*. 2025; 10(7): 7484-7491.
- [8] Yu, F., Shang, J., et al. NeuroSLAM: a brain-inspired SLAM system for 3D environments. *Biological Cybernetics*. 2019; 113(5-6): 515-545.
- [9] Zhang, Y., Trappenberg, T., et al. Continuous attractor neural networks: candidate of a canonical model for neural information representation. *F1000Research*. 2016; 5.
- [10]Finkelstein, A., Las, L., et al. 3-D maps and compasses in the brain. *Annual Review of Neuroscience*. 2016; 39: 171-196.
- [11]Menezes, M.C., Muñoz, M.E., et al. A Multisession SLAM Approach for RatSLAM. *Journal of Intelligent & Robotic Systems*. 2023; 108(4): 61.
- [12]Zeng, T., & Si, B. Cognitive mapping based on conjunctive representations of space and movement. *Frontiers in Neurorobotics*. 2017; 11: 61.
- [13]Silveira, L., Guth, F., et al. An open-source bio-inspired solution to underwater SLAM. *IFAC-PapersOnLine*. 2015; 48: 212-217.
- [14]Michael M., Wyeth, G.F., et al. RatSLAM: a hippocampal model for simultaneous localization and mapping. *IEEE International Conference on Robotics and Automation (ICRA)*. 2004; 403-408.
- [15]Milford, M., & Wyeth, G.F. Mapping a suburb with a single camera using a biologically inspired SLAM system. *IEEE Transactions on Robotics*. 2008; 24(25): 1038-1053.
- [16]Steckel, J., & Peremans, H. BatSLAM: simultaneous localization and mapping using biomimetic sonar. *PLoS ONE*. 2013; 8(1): e54076.
- [17]Yuan, J., Guo, W., et al. A bionic spatial cognition model and method for robots based on the hippocampus mechanism. *Frontiers in Neurorobotics*. 2022; 15: 769829.
- [18]Shen, D., Liu, G., et al. ORB-NeuroSLAM: a brain-inspired 3-D SLAM system based on ORB features. *IEEE Internet of Things Journal*. 2024; 11(7): 12408-12418.
- [19]Chen, Y., Xiong, Z., et al. Brain-inspired multisensor navigation information fusion model based on spatial representation cells. *IEEE Sensors Journal*. 24(11): 18122-18132.
- [20]Yang, C., Xiong, Z., et al. A path integration approach based on multiscale grid cells for large-scale navigation. *IEEE Transactions on Cognitive and Developmental Systems*. 2022; 14(3): 1009-1020.
- [21]Yang, C., Xiong, Z., et al. Brain-inspired multimodal navigation with multiscale hippocampal-

- entorhinal neural network. *IEEE Transactions on Instrumentation and Measurement*. 2024; 73: 8507217.
- [22]Liu, X., Chen, L., et al. A neuro-inspired positioning system integrating MEMS sensors and DTMB signals. *IEEE Transactions on Broadcasting*. 2023; 69(3): 823-831.
- [23]Wang, C., Zhang, T., et al. BrainPy, a flexible, integrative, efficient, and extensible framework for general-purpose brain dynamics programming. *eLife*. 2023; 12: e86365.
- [24]Liu, M., Yurtsever, E., et al. A survey on autonomous driving datasets: statistics, annotation quality, and a future outlook. *IEEE Transactions on Intelligent Vehicles*. 2024; 9(11): 7138-7164.
- [25]Edvardsen, V. Goal-directed navigation based on path integration and decoding of grid cells in an artificial neural network. *Natural Computing*. 2019; 18(1): 13-27.
- [26]Edvardsen, V., Bicanski, A., et al. Navigating with grid and place cells in cluttered environments. *Hippocampus*. 2019; 30(3): 220-232.
- [27]Kymn, C.J., Mazelet, S., et al. Binding in hippocampal-entorhinal circuits enables compositionality in cognitive maps. *International Conference on Neural Information Processing Systems (NeurIPS)*, 2024.
- [28]Dong, X., Ji, Z., et al. Adaptation accelerating sampling-based Bayesian inference in attractor neural networks. *International Conference on Neural Information Processing Systems (NeurIPS)*, 2024.
- [29]Fang, W., Chen Y., et al. SpikingJelly: an open-source machine learning infrastructure platform for spike-based intelligence. *Science Advances*. 2023; 9(40): eadi1480.